ADVANCED MATERIALS
www.advmat.de

Check for updates

2D Electrets of Ultrathin MoO_2 with Apparent Piezoelectricity

Amey Apte, Kosar Mozaffari, Farnaz Safi Samghabadi, Jordan A. Hachtel, Long Chang, Sandhya Susarla, Juan Carlos Idrobo, David C. Moore, Nicholas R. Glavin, Dmitri Litvinov, Pradeep Sharma, Anand B. Puthirath,* and Pulickel M. Ajayan**

Since graphene, a variety of 2D materials have been fabricated in a quest for a tantalizing combination of properties and desired physiochemical behavior. 2D materials that are piezoelectric, i.e., that allow for a facile conversion of electrical energy into mechanical and vice versa, offer applications for sensors, actuators, energy harvesting, stretchable and flexible electronics, and energy storage, among others. Unfortunately, materials must satisfy stringent symmetry requirements to be classified as piezoelectric. Here, 2D ultrathin single-crystal molybdenum oxide (MoO_2) flakes that exhibit unexpected piezoelectric-like response are fabricated, as MoO_2 is centrosymmetric and should not exhibit intrinsic piezoelectricity. However, it is demonstrated that the apparent piezoelectricity in 2D MoO_2 emerges from an electret-like behavior induced by the trapping and stabilization of charges around defects in the material. Arguably, the material represents the first 2D electret material and suggests a route to artificially engineer piezoelectricity in 2D crystals. Specifically, it is found that the maximum out-of-plane piezoresponse is 0.56 pm V^{-1}, which is as strong as that observed in conventional 2D piezoelectric materials. The charges are found to be highly stable at room temperature with a trapping energy barrier of ≈2 eV.

Elemental and compound 2D materials like graphene, black phosphorus, boron nitride, transition metal dichalcogenides (TMDCs), and their various alloys and heterostructures have been exhaustively studied for their exciting physical, chemical, optoelectronic, and mechanical properties.[1–8] Over the recent years, piezoelectricity in these materials has been increasingly explored due to their unique atomically thin nature and large surface area to thickness ratio.[9–14] Piezoelectric materials display reversible interconversion between electricity and mechanical deformation. Accordingly, piezoelectric materials are useful for a variety of sensing, actuating, energy generation and conversion applications.[15–18] Similar to 3D materials, this effect is only possible in 2D materials if they lack inversion symmetry in their crystal structure.[12,19,20]

Various theoretical and experimental investigations have estimated piezoelectric coefficients of 0.2–1 pm V^{-1} for graphene and hBN, 2–10 pm V^{-1} for most TMDCs and 50–200 pm V^{-1} for certain Group IV monochalcogenides and Group V elemental alloys.[12,21–24] The 2H structure of TMDCs lacks inversion center and therefore is capable of showing in-plane piezoelectric output for odd number of layers.[17] Kang et al. realized an out-of-plane piezoelectricity in

Dr. A. Apte,[+] Dr. S. Susarla,[++] Dr. A. B. Puthirath, Prof. P. M. Ajayan
Department of Materials Science and NanoEngineering
Rice University
6100 Main Street, Houston, TX 77005, USA
E-mail: anandputhirath@rice.edu; ajayan@rice.edu

K. Mozaffari, Prof. P. Sharma
Department of Mechanical Engineering
University of Houston
4726 Calhoun Road, Houston, TX 77204, USA
E-mail: psharma@central.uh.edu

The ORCID identification number(s) for the author(s) of this article can be found under https://doi.org/10.1002/adma.202000006.

[+]Present address: Intel Corporation, 5000 W Chandler Blvd, Chandler AZ-85226, USA

[++]Present address: Materials Sciences Division, Lawrence Berkeley National Laboratory, 1 Cyclotron Rd, Berkeley, CA 94720, USA

DOI: 10.1002/adma.202000006

F. S. Samghabadi, Prof. D. Litvinov
Materials Science and Engineering Program
University of Houston
4726 Calhoun Rd, Houston, TX 77204, USA

Dr. J. A. Hachtel, Dr. J. C. Idrobo
Center for Nanophase Materials Sciences
Oak Ridge National Laboratory
Oak Ridge, TN 37831, USA

Dr. L. Chang, Prof. D. Litvinov
Department of Electrical and Computer Engineering
University of Houston
Houston, TX 77204, USA

Dr. D. C. Moore, Dr. N. R. Glavin
Materials and Manufacturing Directorate
Air Force Research Laboratory
Wright-Patterson AFB, Dayton, OH 45433, USA

Prof. P. Sharma
Department of Physics
University of Houston
3507 Cullen Blvd, Houston, TX 77204, USA

 © 2020 WILEY-VCH Verlag GmbH & Co. KGaA, Weinheim

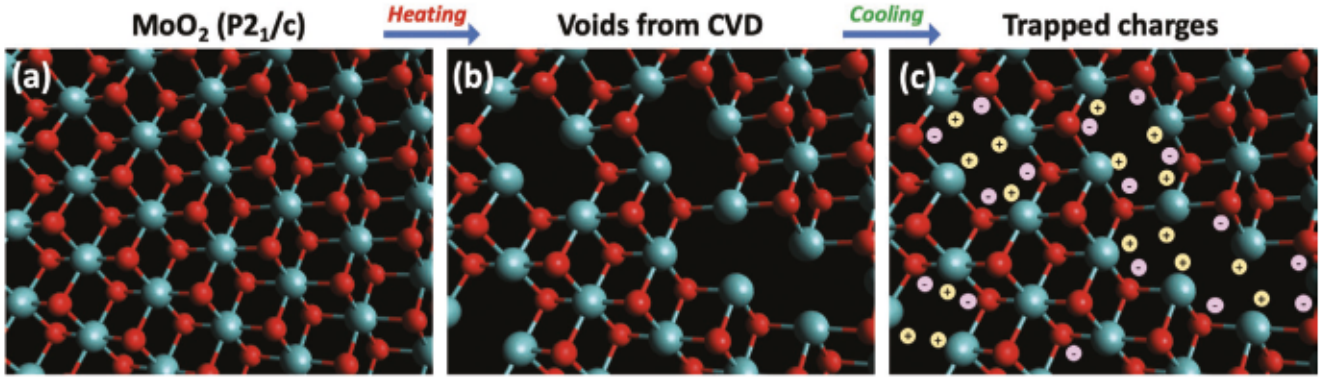

Figure 1. Schematic of an electret formation: a) Normal MoO_2 crystal structure comprising Mo (cyan)–O (red) octahedra. b,c) Void formation during CVD synthesis at high temperature (b), giving rise to charges trapped during the cooling phase post-deposition (c).

2D $MoTe_2$ flakes by means of artificial corrugation.[25] Guo et al. demonstrated the importance of functionalizing the surfaces of various 2D nitride materials for generating piezoelectricity.[26] Xue et al. obtained an out-of-plane piezoelectric coefficient of 0.34 pm V^{-1} for monolayer α-In_2Se_3, which itself contains odd (five) number of atomic layers.[27] Another interesting category of 2D materials are Janus monolayers, which can show stronger piezoelectricity than their standard TMDC counterparts.[28] These developments bring to fore artificial approaches to create piezoelectricity in materials that are not intrinsically so. A rather notable example of this was the proposal for making graphene ribbon piezoelectric through exploitation of flexoelectricity and engineering precise defects.[29] Unfortunately, such approaches are difficult to realize in practice.

In this work, we unequivocally demonstrate the piezoelectric response of 2D molybdenum dioxide (MoO_2) flakes. MoO_2 crystallizes in a monoclinic $P2_1/c$ structure which is centrosymmetric[30]; this along with delocalizing of electrons across differing Mo—O bond lengths leads to an unusual metallic-like conductivity thereby precluding expectations of conventional piezoelectric behavior. The MoO_2 flakes grown via chemical vapor deposition (CVD) exhibit large size up to tens of micrometers, ultrathin (≈6 nm) and single crystalline with well-defined edges. The crystal structure of the MoO_2 is confirmed via Raman spectroscopy and X-ray diffraction, and the microstructure of the flakes is observed to possess a high concentration of vacancies and defects through atomic-resolution imaging in a scanning transmission electron microscope (STEM). Piezoresponse force microscopy (PFM) is utilized to image the MoO_2 system along with switching spectroscopy to quantify amplitude and phase loops showing strong out-of-plane piezoelectric coefficient of 0.56 pm V^{-1}.

We systematically investigate the mechanism underpinning the apparent piezoelectric behavior of MoO_2 and conclude its origins to the formation of the so-called electret state. We propose that the 2D MoO_2 flakes in this work, synthesized via CVD at high temperature, contain defects and voids which act as prime spots for trapping charges before the growth process completes and sample is cooled down to room temperature. In short, the 2D flakes possess frozen dipoles. Electret behavior is confirmed by performing charge-leakage studies where the samples are heated for an extended period of time giving rise to a nonreversible loss of piezoelectricity.

We hypothesize that our fabricated 2D material is an "electret" and this is the key mechanism underpinning its apparent piezoelectric behavior. Electret materials are dielectric materials with embedded immobile or trapped charges and dipoles as shown schematically in **Figure 1**. While the key notions pertaining to electrets appear to originate more than a century ago, its technological implication became only evident in the eighties in the context of polymer foams. Numerous groups fabricated soft polymer foams containing large dipoles inserted on the void surfaces by the process of corona charging.[31–35] These electrets were found to exhibit large apparent piezoelectric coefficients; for example as large as 1200 pC N^{-1}, which is nearly six times larger than the arguably most often used ferroelectric piezoelectric ceramic: lead zirconium titanate.[36] Recent theoretical modeling has well-explained the origins of the apparent piezoelectric, flexoelectric, and pyroelectric behavior in electrets (in otherwise nonpiezoelectric) materials due to the interaction of Maxwell stress (or electrostriction), deformation nonlinearity, and the presence of the charges or dipoles.[37–41]

To date, although electrets have been demonstrated for soft polymer foams, there is no example of a 2D electret material. In particular, a key aspect of electret is that charges must be stabilized since the electret state is metastable and the charges have a tendency to decay. Well-fabricated foams often have stabilized life (at room temperature) for decades. Notably, the decay is significantly hastened at high temperature and annealing studies provide a definitive confirmation of whether a material is an electret or not. Based on experimental observations of the microstructure, we believe that charges and dipoles trap in the voids and defects of ultrathin MoO_2 flakes thus creating an electret state (Figure 1).

In order to model and interpret the piezoresponse of the ultrathin MoO_2 flakes, we estimated mechanical properties such as Young's modulus and hardness via nanoindentation measurements. Observing the low thickness of the flakes, to nullify the substrate effects, the penetration length of intender probe was limited to much lesser values compared to the thickness of the sample. The results of the measurements are displayed in Figures S1–S3 in the Supporting Information. The reduced modulus (E_R*) and hardness (H) were measured to be 103.25 and 2.13 GPa, respectively. This is significantly lower than the known elastic properties of the material (E_1 = 471.41 GPa).[42,43] Our microstructural analysis shows significant fraction of voids,

© 2020 WILEY-VCH Verlag GmbH & Co. KGaA, Weinheim

which is attributed to the lower elastic measurement. The relation between the elastic properties of a porous material may be estimated through the following homogenization framework[44]

$$\frac{k^*}{k_1} = 1 + \frac{v_f\,[k]}{k_1 + \alpha_1(1-v_f)\,[k]} \tag{1}$$

$$\frac{\mu^*}{\mu_1} = 1 + \frac{v_f\,[\mu]}{\mu_1 + \beta_1(1-v_f)\,[\mu]} \tag{2}$$

Here, k_i and μ_i are the bulk and shear moduli of the material, subscripts 1 and 2 are referred to the matrix and void, the superscript * is referred to the effective properties of the porous media, and v_f is the volume fraction of the voids. Here, [_] denotes the jump in the material properties, i.e., $[\mu] = \mu_2 - \mu_1$. α_1 and β_1 are dimensionless parameters given by[44]

$$\alpha_1 = \frac{3k_1}{3k_1 + 4\mu_1} \tag{3}$$

$$\beta_1 = \frac{6}{5}\,\frac{k_1 + 2\mu_1}{3k_1 + 4\mu_1} \tag{4}$$

These relations provide us with an approximation for the void fraction, which is found to be in the range of $v_f = 0.29$. In short, the fabricated material is highly defective.

We now proceed to calculate the amount of the charge trapped in the voids, which would be achieved by assuming that the voids accumulate in layers of thickness H_a in between of the MoO_2 layers with the thickness of H_m (the ratio of the layer thickness corresponds to the volume fraction). Following an approach outlined in ref. [37], we obtain the following expression for apparent or effective piezoelectricity of the 2D electret. (The detailed derivation of this relation is shown in the Supporting Information.)

$$d_{\text{eff}} = \frac{-\varepsilon_0\varepsilon_m H_a H_m q_0}{v_f E^*(\varepsilon_0 H_m + \varepsilon_m H_a)^2} \tag{5}$$

The piezoelectric coefficient was measured both for untreated samples as well as ones that were heated for 3 days at 250 °C. In an intrinsic piezoelectric, heating should cause no discernible permanent change in its piezoelectric behavior. In our experiments, however, the piezoelectric coefficient before heating, $d_i^{\text{eff}} = 0.56\ \text{pC N}^{-1}$ drops to $d_f^{\text{eff}} = 0.072\ \text{pC N}^{-1}$. Using the state model, we estimate that the amount of charge density before heating in the range of $q_0^{(1)} = -0.070$ reduced to $q_0^{(2)} = -0.009\ \text{C m}^{-2}$ after heating. The range is due to the error bar in our measurement of the elastic properties and hence the estimate of volume fraction of the voids. With the knowledge of the time and temperature, which caused the aforementioned charge leakage, we may also estimate the current of the charge release from the material $I(t)$ and the trapping energy barrier E_a from[45]

$$I(t) = n_0\, e^{-\nu\, e^{-E_a/k_bT}}\, .\nu\, e^{-E_a/k_bT} \tag{6}$$

where n_0 is the amount of charge at the beginning, t is the time of heating, ν is defined as attempt of electron to escape frequency with unit of s^{-1} and the acceptable range for it is reported from 10^{14} to $10^{12}\ s^{-1}$, k_b is the Boltzmann constant, and T is the absolute temperature. Since effective piezoelectric coefficient is directly proportional to the charge induced current, we can conclude that

$$d^{\text{eff}} \propto n_0 e^{-\nu\, e^{-E_a/k_bT}}\, .\nu\, e^{-E_a/k_bT} \tag{7}$$

From this, we estimate the energy barrier E_a by using the following relation

$$\frac{d_i^{\text{eff}}}{d_f^{\text{eff}}} = e^{\nu\, e^{-E_a/k_bT}} \tag{8}$$

We find that $E_a = 1.77522$ to 1.98283 eV based on the choice of ν. With the energy barrier at hand, we may now estimate how stable the electret state is at room temperature. Simply put, with the estimated energy barrier, the electret state will last close to a year at 200 °C but will rapidly destabilize above it. However, at room temperature or even up to 100 °C, nearly infinite life is predicted.

Figure 2a describes the synthesis and characterization of the ultrathin MoO_2 flakes. As described in the experimental details, the flakes grow directly on the 285 nm SiO_2 layer on top of Si substrate. The presence of Ar/H_2 carrier gas provides a reducing environment for the $(NH_4)_2MoO_4$ vapors which convert the Mo^{6+} ions to Mo^{4+} in MoO_2 at elevated temperatures according to the following chemical reaction

$$(NH_4)_2\,MoO_4 + H_2\,(Ar) \rightarrow MoO_2 + 2H_2O + 2NH_3\uparrow \tag{9}$$

The photomicroscopy image (50×) of as-grown ultrathin MoO_2 flakes on SiO_2/Si substrate is presented in Figure 2b. The two peaks at 302 and 520 cm^{-1} seen in the Raman spectra (Figure 2c) originate from the underlying Si substrate. The MoO_2 peaks are found at 122, 201, 228, 346, 361, 458, 465, 495, 571, 587, and 744 cm^{-1}. Of these, the bands at 587 and 744 cm^{-1} are characteristic of MoO_2 and attributed to the Mo—O bond stretching vibrations.[46]

The crystal structure of the as-grown flakes was studied with grazing incidence X-ray diffraction (GI-XRD). In Figure 2d, the observed peaks were indexed to the Tugarinovite phase with monoclinic $P2_1/c$ structure (ICDD DB# 04-007-9726) with calculated lattice parameters a = 5.587 Å, b = 4.836 Å, c = 5.605 Å, and β = 120.95°. Atomic force microscopy (AFM) was performed to determine the topography and thickness of the flakes. Figure 2e shows AFM image of a single crystal flake. The thickness was measured to be 6 nm, corresponding to ten atomic layers. Further AFM measurements are included in Figure S2 in the Supporting Information. In order to determine the chemical bonding states, X-ray photoelectron spectra (XPS) of the samples were recorded. Figure 2f,g shows the molybdenum 3d and oxygen 1s core level spectra along with the fitted peaks. All spectra were referenced by adventitious carbon 1s peak at 284.8 eV (not shown). For Mo 3d, three pairs of doublets ($3d_{5/2}$ and $3d_{3/2}$) are fitted at 229.5 and 232.9, 231.5 and 234.6, and 232.6 and 236 eV, respectively. The first two pairs are due to the Mo^{4+} oxidation state as expected in the MoO_2 stoichiometry whereas

© 2020 WILEY-VCH Verlag GmbH & Co. KGaA, Weinheim

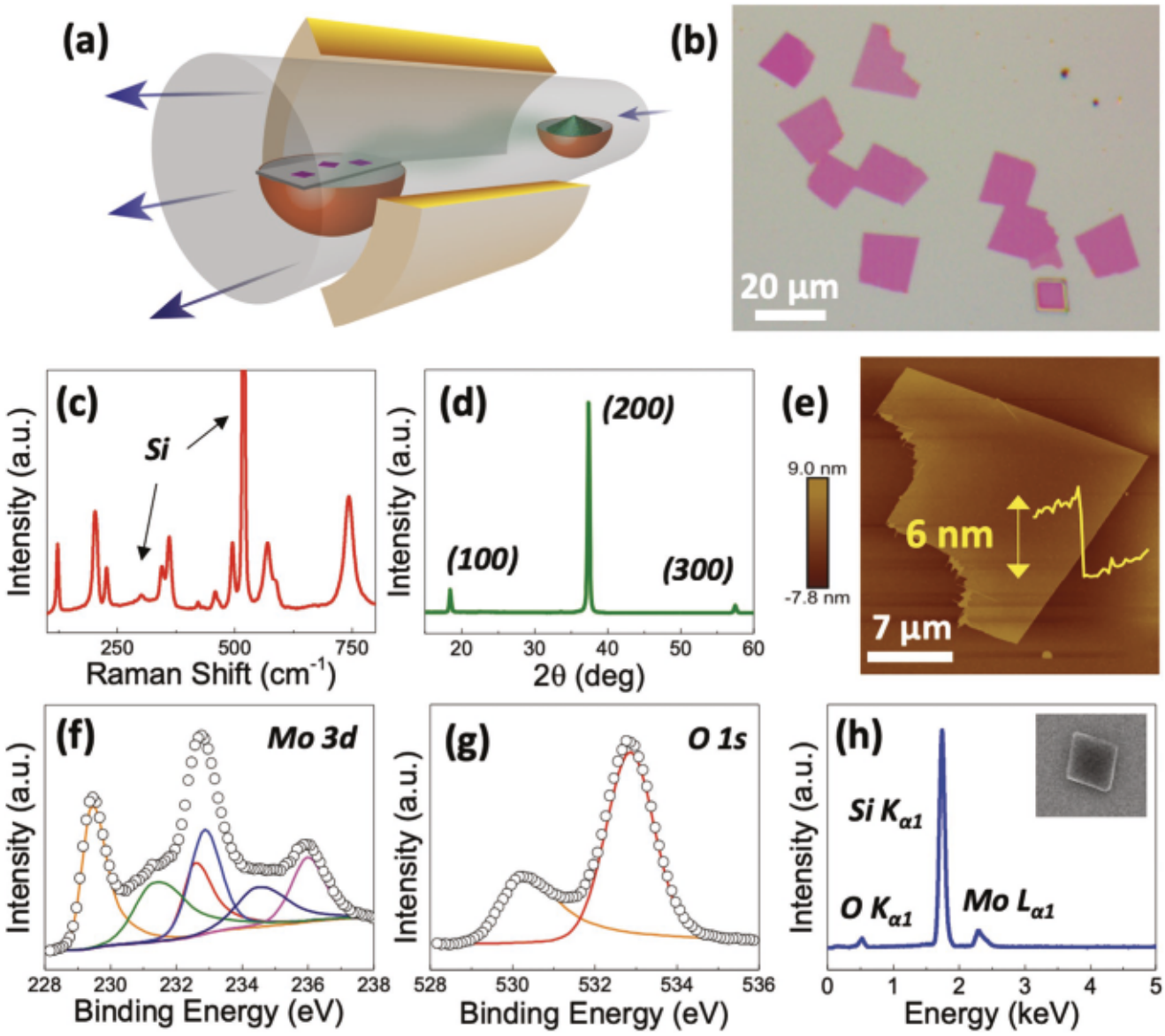

Figure 2. Characterization of synthesized MoO_2 flakes: a) Schematic of CVD synthesis. b) Optical microscopy image (50×) of as-grown ultrathin MoO_2 flakes on SiO_2/Si substrate. c) Raman spectrum of single MoO_2 flake. d) Grazing-incidence X-ray diffraction pattern indexed to $P2_1/c$ monoclinic structure. e) Atomic force microscopy image of single flake showing ultrathin nature (≈6 nm). f,g) X-ray photoelectron spectra for Mo 3d and O 1s regions. h) EDAX spectra of single MoO_2 flake (inset, SEM image) showing Mo and O characteristic X-ray lines; the Si peak originates from the underlying substrate.

the third is due to Mo^{6+}, which can be attributed to the presence of trioxide pockets at/near the voids of the lattice as well as some small surface oxidation/residue on the substrates apart from the flakes. However, MoO_3 is not present extensively in the flakes ass there is no corroboration in the Raman data for key modes at 285, 666, and 823 cm^{-1}, which are missing in Figure 2c.[46] For the oxygen 1s spectra, there are two peaks at 530.4 and 532.9 eV which can be attributed to the oxide bonds found in MoO_2 and SiO_2, respectively. The chemical presence of the elements is further verified by energy-dispersive X-ray spectroscopy (scanning electron microscopy (SEM)–EDAX) shown in Figure 2h. The inset shows SEM image of a single MoO_2 flake from which the spectrum was acquired. The spectrum itself contains peaks at 0.52, 1.74, and 2.28 keV, 2.36 keV attributed to the O $K_{α1}$, Si $K_{α1}$, and Mo $L_{α1}/L_{β1}$ transitions, respectively, and thus confirming the elemental composition of the sample.

The MoO_2 flakes are transferred to TEM grids to examine the atomic-resolution structure of the material. **Figure 3**a shows a high-angle annular dark-field (HAADF) STEM image of monoclinic $P2_1/c$ MoO_2 in the [201] projection, which is characterized by parallel rows of Mo doublets. HAADF imaging utilizes *Z*-contrast, where the measured intensity is determined by the number of atoms and the atomic number of the elements in each column. Here, significant variation in the HAADF intensity is readily observed between the sites in the Mo doublets and between adjacent Mo doublets across the entire imaged region. This high level of variation in the HAADF intensity indicates

© 2020 WILEY-VCH Verlag GmbH & Co. KGaA, Weinheim

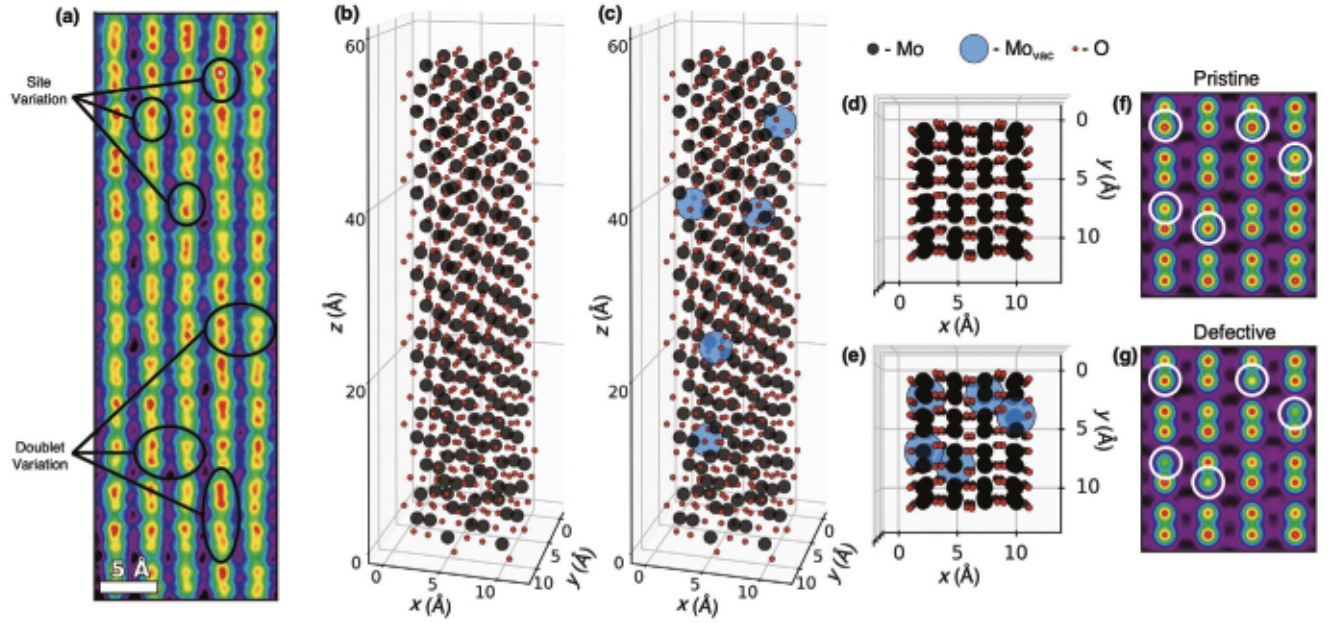

Figure 3. HAADF-STEM imaging of an MoO_2 flake. a) Atomic-resolution HAADF image of the edge of a MoO_2 flake showing the [201] projection of the monoclinic structure, showing extensive intensity variation in the Mo columns and doublets. b,c) 3D scatter plots of ≈6 nm slab of MoO_2 without defects (b) and with 5 embedded vacancies (c). d,e) [201] projections of scatter plots in (b) and (c), respectively. f,g) Simulated HAADF images of the pristine (f) and defective (g) MoO_2 slabs, showing influence of individual voids/vacancies (circles denote Mo columns possessing vacancies in defective structure).

variations in the stoichiometry across the different atomic-columns, which is consistent with the vacancy-rich single-crystal structure needed to form an ultrathin electret material (additional STEM analysis and validation is included in Figure S4 in the Supporting Information.

While the precise location and nature of the defects cannot be directly determined from the HAADF image, we use STEM simulations to demonstrate that it is consistent with a high vacancy/void concentration in the MoO_2 flakes. Figure 3b,c shows scatter plots of a 5.7 nm thick flake of MoO_2 both without vacancies (Figure 3b) and with 5 vacancies randomly embedded in the structure (Figure 3c). The [201] projections of the scatter plots, which would match the orientation of the STEM image, are shown in Figure 3d,e, respectively. Here, the vacancies are denoted by large blue circles, to show that in these models there is at most 1 vacancy per column, and that all the vacancies are at different heights in the projected direction. The simulated HAADF-STEM images for each of these slabs is shown in Figure 3f,g, respectively. The atomic columns which possess vacancies in the defective structure are marked in the simulated images with and without vacancies for comparison, and it can be observed that the influence of individual vacancies is clearly observable for ≈6 nm flakes.

It is important to note that there is no a priori mechanism to distinguish between a vacancy at the surface of the flake and void in the bulk. However, the abundance of atomic-scale variation in the HAADF intensity across the entire flake (as observed in Figure 3a and Figure S4d in the Supporting Information) indicates a large number of defects that we believe is more likely to be spread throughout the bulk than concentrated entirely at the surface. Thus, the STEM is indicative of a large number of vacancies and voids in the MoO_2 lattice.

The presence of defects and voids in the microstructure of the ultrathin MoO_2 flakes is explained due to chemical vapor deposition, which has a well-known tendency to create defects during nucleation and growth processes[47–49] However, the presence of defects in this ultrathin structure can give rise to unexpected behavior, i.e., ferroelectrets. Accordingly, a sample of MoO_2 on SiO_2/Si substrate was investigated by PFM. Piezoresponse force microscopy has shown to be a powerful tool for the characterization of piezoelectric materials on the nanoscale. Alignment of electric dipoles in a piezoelectric material due to the application of an external electric field physically shows up as material elongation or contraction. In PFM, the surface electromechanical deformation is detected as the first harmonic component of a conductive tip deflection, oscillating in contact with the surface. The deflection amplitude is proportional to the converse piezoelectric coefficient and the phase yields information about polarization direction below the tip.[50–52] Here, dual AC resonance tracking (DART)-PFM method was employed to study the bias-induced surface deformation of samples. **Figure 4**a–c shows the typical PFM data recorded on a single MoO_2 flake at 10 V bias, i.e., topography, deflection amplitude, and phase, respectively. As expected, the ultrathin nature of the flake is confirmed from the topography (≈8.7 nm thickness).

The thick central region in the topographical image in Figure 4a is merely organic impurity unrelated to the MoO_2 as seen by the otherwise smooth nature of the flake, and also does not show up in the PFM data. The maximum PFM deflection amplitude as seen in Figure 4b was measured as ≈0.4 nm. Therefore, the converse piezoelectric coefficient (d_{33}) turns out to be 0.56 pm V^{-1} (divided by applied bias of 10 V and a quality factor of 71.2). The PFM phase signal also undergoes changes when the tip is over the flake as evident from Figure 4c;

© 2020 WILEY-VCH Verlag GmbH & Co. KGaA, Weinheim

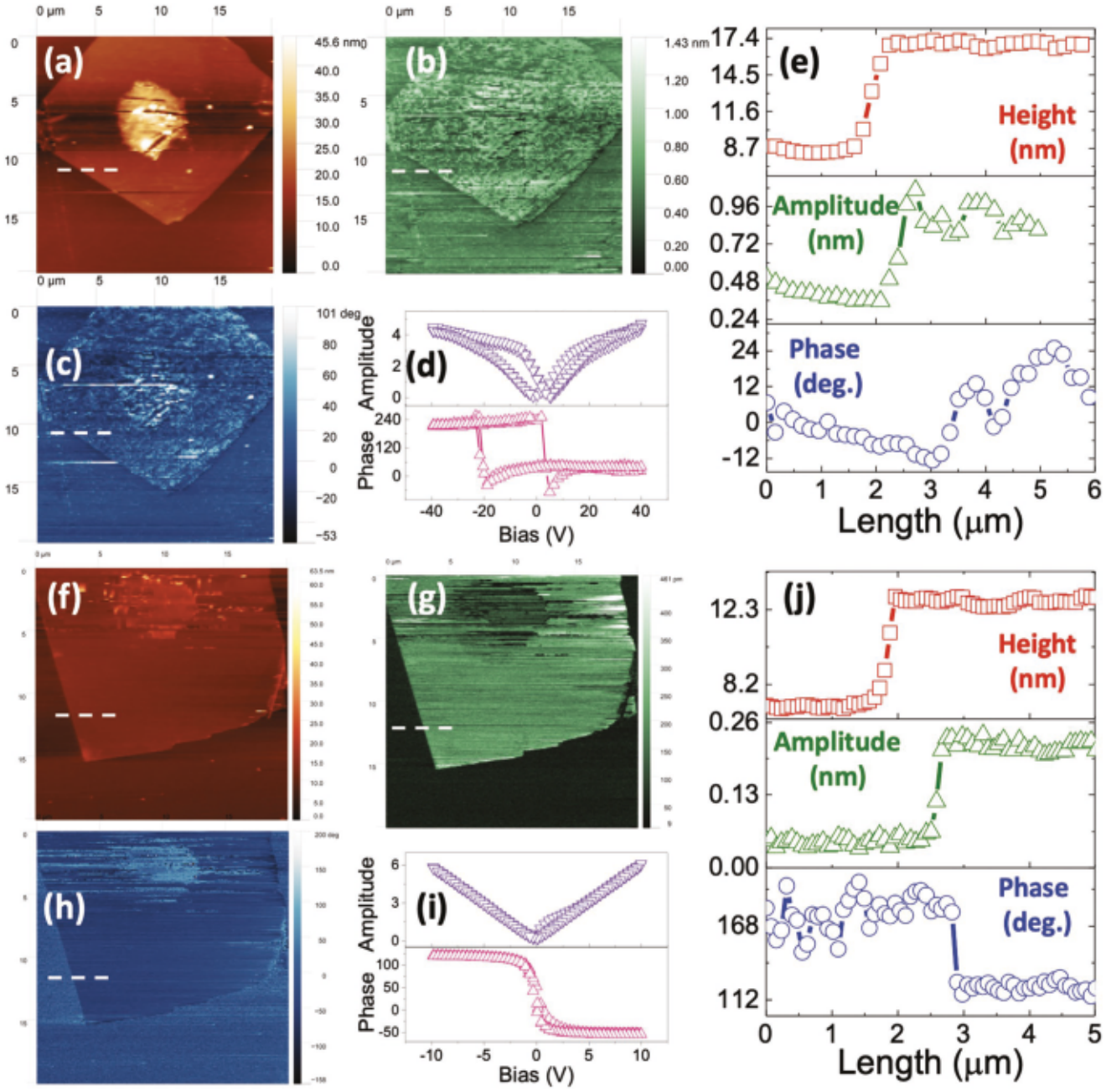

Figure 4. PFM experiments on MoO_2 flakes. a) Topography, b) PFM amplitude, and c) PFM phase maps of single MoO_2 flake. d) S-PFM showing strong hysteresis in PFM amplitude ($\times 10^{-9}$ m) and phase signals. e) Line profiles extracted from (a)–(c) of the respective maps. f) Topography, g) PFM amplitude ($\times 10^{-9}$ m), and h) PFM phase maps of heat-treated MoO_2 single flake (250 °C, 3 days) showing better homogeneity in the response signal. i) S-PFM showing negligible hysteresis in amplitude and phase due to dissipation of charges from the flakes after heat treatment. j) Line profiles extracted from (f)–(h) of the respective maps.

however, these changes are not uniform over the entire flake. Further, switching spectroscopy PFM (S-PFM) was performed at points over the MoO_2 flake by holding the position of the tip constant, while superimposing a triangle–square waveform bias to ac driving voltage. PFM spectroscopy generates local hysteresis loops, which provides valuable information about electromechanical behavior of piezoelectric materials like nucleation biases, coercive voltage variations and domain-wall pinning on the nanoscale.[50,53]

The resulting variation in the PFM tip deflection amplitude and phase is plotted as a function of the applied bias in Figure 4d. The characteristic butterfly loop in the PFM amplitude and the hysteresis in the phase signal are readily apparent (lower curve) and is believed to arise from the ferroelectret response to the applied field. Extended piezoresponse and Kelvin probe force microscopy (KPFM) studies are performed on the flakes in order to alleviate the chance of seeing hysteresis as a result of charge injection from the PFM tip. The

© 2020 WILEY-VCH Verlag GmbH & Co. KGaA, Weinheim

results are provided inFigures S7–S11 in the Supporting Information.[54–56] Since electrets are accumulated charges due to the peculiar defect-based microstructure of the MoO_2 flakes, they are not thermodynamically stable. Therefore, the sample was heated at elevated temperature (250 °C) for three days in an inert environment (to prevent unwanted oxidation) and reexamined with PFM. Annealed flakes are characterized structurally and electrically, and the analysis details are appended in SI (Figure S6a–d, Supporting Information). Figure 4f–h shows the topography, and PFM amplitude and phase maps of a single MoO_2 flake postheat treatment. In this case, we can see that while the PFM response of the flake has reduced, it is now more consistent and homogenous across the whole flake region—the max deflection amplitude (≈0.15 nm) has reduced, amounting to a deflection coefficient (d_{33}) of 0.072 pm V^{-1} (divided by applied bias 10 V and quality factor 207.47), whereas the phase signal shows clear jump of ≈56° between the flake and the substrate. This is due to the extended heat treatment mobilizing the electrets and promoting homogeneity as well as dissipation from the middle layers of the flake up toward the surface. Figure 4i shows the result of S-PFM carried out on the MoO_2 flake postheat treatment, in similar fashion as described previously—we see no superimposed butterfly loop for the PFM amplitude (upper curve) and a complete lack of hysteresis behavior in the phase response (lower curve) of the heat-treated sample.

Ultrathin MoO_2 flakes of up to 20 µm lateral sizes were grown on SiO_2/Si substrates via versatile method of chemical vapor deposition. Raman spectroscopy and X-ray diffraction identified the characteristic monoclinic structure whereas atomic force microscopy showed the flakes having between 6 and 10 nm thickness. X-ray photoelectron spectroscopy and energy-dispersive X-ray spectroscopy showed the chemical presence of Mo and O elements whereas HAADF-STEM showed the high concentration of microscopic defects (voids, vacancies, etc.) in the MoO_2 lattice. PFM was utilized to demonstrate the electret-based effects in individual MoO_2 flakes with an out-of-plane coefficient of 0.56 pm V^{-1}. Heating at 250 °C for 3 days reduced the ferroelectric behavior as observed via PFM switching spectroscopy and confirming the electret hypothesis. The work demonstrates a route to artificially engineering piezoelectricity in nonpiezoelectric 2D materials.

Experimental Section

Synthesis: Ultrathin molybdenum dioxide (MoO_2) flakes were grown via chemical vapor deposition. Few grams of ammonium molybdate ($(NH_4)_2MoO_4$, Sigma-Aldrich, 99.9%) powder was placed in a porcelain crucible kept at the center of a quartz tube furnace. SiO_2/Si substrates (precleaned with acetone and isopropyl alcohol) were placed face-down on top of the powder. A mixture of 85% Ar and 15% H_2 gas was flown to purge the tube, followed by ramping the furnace from room temperature to 600 °C in 20 min. This temperature was held for 20 min followed by cooling down up to 500 °C at which the furnace hood was opened to quench the tube down to room temperature. The MoO_2 flakes were obtained on the inverted side of the substrates as observed in an optical microscope. For HAADF-STEM imaging, the flakes were transferred to Quantifoil grids via coating of PMMA layer on top of as-grown substrates followed by wet etching in 2 M KOH. After being transferred, the PMMA layer was dissolved in acetone and isopropyl alcohol followed by baking at 100 °C.

Characterization: Raman spectra and spatial maps were recorded on a Renishaw inVia spectrometer with 532 nm laser at 10% incident intensity and 10 s acquisition time. X-ray diffraction patterns were measured on a Rigaku SmartLab XRD with Cu Kα radiation (1.54 Å) in 2Theta/Omega configuration. AFM images were recorded on a Bruker Multimode 8 in Scanasyst mode. XPS spectra were obtained via PHI Quantera II with monochromated Al Kα at 1486.6 and 26 eV pass energy. Scanning electron microscopy images and EDAX spectra were obtained on a FEI Quanta 400 ESEM at 5 and 30 kV, respectively. STEM images were recorded on a Nion UltraSTEM 100 operating at 60 kV, with a convergence angle of 32 mrad. The HAADF detector possessed an inner collection angle of ≈80 mrad and an outer collection angle of ≈200 mrad. STEM simulations were performed using Prismatic, with the same detector and probe parameters as used in the ≈13 unit-cell thick MoO_2 slab oriented in the [201] projection, with a slice thickness of 0.05 Å, a probe step-size of 0.1 Å, and no interpolation.[57,58] The STEM was equipped with a Gatan Enfina electron energy-loss (EEL) spectrometer. The EELS experiments were performed with a convergence semiangle of 30 mrad, and an EELS collection semiangle of 48 mrad. A Hysitron TI 980 Tribo Indenter having Berkovich probe with radius of curvature 150 nm was employed for the Nanoindentation experiments. Single indents were performed using a basic QS trapezoid load function (max load 40 µN). PFM was done with ASYLUM Research probe model "ASYELEC-01-R2" (MFP-3D origin+ Asylum Research AFM by Oxford Instruments with a silicon tip coated with Ti/Ir (5/20)). The probe spring constant and lever air resonance frequency were 2.8 N m^{-1} and 75 kHz, respectively. The resonance frequency of the tip during measurement was 360 kHz on average. KPFM was measured on a Bruker Dimension Icon in PeakForce KPFM (frequency modulated) mode using a PFQNE-AL probe. Surface potential was applied via back gating for 15 min and the transient response was recorded over a single line with a 50 nm interleave lift at 977 mHz or 2.04 s per line for 11.5 min. Values over the MoO_2 region were then averaged.

Supporting Information

Supporting Information is available from the Wiley Online Library or from the author.

Acknowledgements

This material was based upon work supported by the Air Force Office of Scientific Research under award number FA9550-18-1-0072 (P.M.A, A.A., and A.B.P). P.S. gratefully acknowledges support from true University of Houston M.D. Anderson Professorship. Microscopy research performed as part of a user proposal at Oak Ridge National Laboratory's Center for Nanophase Materials Sciences (CNMS), which is a U.S. Department of Energy, Office of Science User Facility. N.G. thanks the support of the Air Force Office of Scientific Research grant FA9550-19RYCOR050.

Conflict of Interest

The authors declare no conflict of interest.

Author Contributions

A.A. synthesized the samples and carried out characterization with the help of A.B.P. and S.S. J.A.H. and J.C.I. performed STEM experiments and analysis. A.A., A.B.P., F.S., L.C., and D.L. carried out PFM imaging and analysis. K.M. and P.S. carried out theoretical calculations and modeling. D.C.M. and N.R.G. carried out KPFM experiments. P.S. and P.M.A. advised the concept and research. All authors contributed in writing the manuscript.

© 2020 WILEY-VCH Verlag GmbH & Co. KGaA, Weinheim

Keywords

2D electrets, 2D materials, defects, piezoelectricity, trapped charges

Received: January 1, 2020
Revised: April 6, 2020
Published online: May 6, 2020

[1] A. K. Geim, K. S. Novoselov, *Nat. Mater.* **2007**, *6*, 183.
[2] K. S. Novoselov, D. Jiang, F. Schedin, T. J. Booth, V. V. Khotkevich, S. V. Morozov, A. K. Geim, *Proc. Natl. Acad. Sci. USA* **2005**, *102*, 10451.
[3] L. Li, Y. Yu, G. J. Ye, Q. Ge, X. Ou, H. Wu, D. Feng, X. H. Chen, Y. Zhang, *Nat. Nano* **2014**, *9*, 372.
[4] N. Alem, R. Erni, C. Kisielowski, M. D. Rossell, W. Gannett, A. Zettl, *Phys. Rev. B* **2009**, *80*, 155425.
[5] B. Radisavljevic, A. Radenovic, J. Brivio, V. Giacometti, A. Kis, *Nat. Nanotechnol.* **2011**, *6*, 147.
[6] G. R. Bhimanapati, Z. Lin, V. Meunier, Y. Jung, J. Cha, S. Das, D. Xiao, Y. Son, M. S. Strano, V. R. Cooper, L. Liang, S. G. Louie, E. Ringe, W. Zhou, S. S. Kim, R. R. Naik, B. G. Sumpter, H. Terrones, F. Xia, Y. Wang, J. Zhu, D. Akinwande, N. Alem, J. A. Schuller, R. E. Schaak, M. Terrones, J. A. Robinson, *ACS Nano* **2015**, *9*, 11509.
[7] V. Kochat, A. Apte, J. A. Hachtel, H. Kumazoe, A. Krishnamoorthy, S. Susarla, J. C. Idrobo, F. Shimojo, P. Vashishta, R. Kalia, A. Nakano, C. S. Tiwary, P. M. Ajayan, *Adv. Mater.* **2017**, *29*, 1703754.
[8] S. Susarla, A. Kutana, J. A. Hachtel, V. Kochat, A. Apte, R. Vajtai, J. C. Idrobo, B. I. Yakobson, C. S. Tiwary, P. M. Ajayan, *Adv. Mater.* **2017**, *29*, 1702457.
[9] C. J. Brennan, R. Ghosh, K. Koul, S. K. Banerjee, N. Lu, E. T. Yu, *Nano Lett.* **2017**, *17*, 5464.
[10] T. Wu, H. Zhang, *Angew. Chem., Int. Ed.* **2015**, *54*, 4432.
[11] M. López-Suárez, M. Pruneda, G. Abadal, R. Rurali, *Nanotechnology* **2014**, *25*, 175401.
[12] K.-A. N. Duerloo, M. T. Ong, E. J. Reed, *J. Phys. Chem. Lett.* **2012**, *3*, 2871.
[13] J. Xiao, H. Zhu, Y. Wang, W. Feng, Y. Hu, A. Dasgupta, Y. Han, Y. Wang, D. A. Muller, L. W. Martin, P. Hu, X. Zhang, *Phys. Rev. Lett.* **2018**, *120*, 227601.
[14] M. Zelisko, Y. Hanlumyuang, S. Yang, Y. Liu, C. Lei, J. Li, P. M. Ajayan, P. Sharma, *Nat. Commun.* **2014**, *5*, 4284.
[15] N. Jena, Dimple, S. D. Behere, A. De Sarkar, *J. Phys. Chem. C* **2017**, *121*, 9181.
[16] S. A. Han, J. Lee, J. Lin, S.-W. Kim, J. H. Kim, *Nano Energy* **2019**, *57*, 680.
[17] W. Wu, L. Wang, Y. Li, F. Zhang, L. Lin, S. Niu, D. Chenet, X. Zhang, Y. Hao, T. F. Heinz, J. Hone, Z. L. Wang, *Nature* **2014**, *514*, 470.
[18] S. K. Kim, R. Bhatia, T.-H. Kim, D. Seol, J. H. Kim, H. Kim, W. Seung, Y. Kim, Y. H. Lee, S.-W. Kim, *Nano Energy* **2016**, *22*, 483.
[19] N. Kumar, S. Najmaei, Q. Cui, F. Ceballos, P. M. Ajayan, J. Lou, H. Zhao, *Phys. Rev. B* **2013**, *87*, 161403.
[20] M. N. Blonsky, H. L. Zhuang, A. K. Singh, R. G. Hennig, *ACS Nano* **2015**, *9*, 9885.
[21] M. T. Ong, E. J. Reed, *ACS Nano* **2012**, *6*, 1387.
[22] Z. Chang, W. Yan, J. Shang, J. Z. Liu, *Appl. Phys. Lett.* **2014**, *105*, 023103.
[23] H. Yin, J. Gao, G.-P. Zheng, Y. Wang, Y. Ma, *J. Phys. Chem. C* **2017**, *121*, 25576.
[24] R. Fei, W. Li, J. Li, L. Yang, *Appl. Phys. Lett.* **2015**, *107*, 173104.
[25] S. Kang, S. Jeon, S. Kim, D. Seol, H. Yang, J. Lee, Y. Kim, *ACS Appl. Mater. Interfaces* **2018**, *10*, 27424.
[26] Y. Guo, H. Zhu, Q. Wang, *ACS Appl. Mater. Interfaces* **2019**, *11*, 1033.
[27] F. Xue, J. Zhang, W. Hu, W.-T. Hsu, A. Han, S.-F. Leung, J.-K. Huang, Y. Wan, S. Liu, J. Zhang, J.-H. He, W.-H. Chang, Z. L. Wang, X. Zhang, L.-J. Li, *ACS Nano* **2018**, *12*, 4976.
[28] L. Dong, J. Lou, V. B. Shenoy, *ACS Nano* **2017**, *11*, 8242.
[29] S. Chandratre, P. Sharma, *Appl. Phys. Lett.* **2012**, *100*, 023114.
[30] L. E. Conroy, L. Ben-Dor, R. Kershaw, A. Wold, *Inorganic Syntheses: Nonmolecular Solids*, Vol. *30*, John Wiley & Sons, Inc., New York **1995**.
[31] S. Bauer, R. Gerhard-Multhaupt, G. M. Sessler, *Phys. Today* **2004**, *57*, 37.
[32] R. Danz, *Electrets, Topics in Applied Physics*, Vol. *33*, Springer Verlag, Berlin **1980**.
[33] G. M. Sessler, J. Hillenbrand, in *10th Int. Symp. on Electrets (ISE 10)*, IEEE, Piscataway, NJ, USA **1999**, pp. 261–264.
[34] G. Buchberger, R. Schödiauer, S. Bauer, *Appl. Phys. Lett.* **2008**, *92*, 123511.
[35] M. Wegener, S. Bauer, *ChemPhysChem* **2005**, *6*, 1014.
[36] J. Hillenbrand, G. M. Sessler, *J. Appl. Phys.* **2008**, *103*, 074103.
[37] Q. Deng, L. Liu, P. Sharma, *Phys. Rev. E* **2014**, *90*, 12603.
[38] Z. Alameh, Q. Deng, L. Liu, P. Sharma, *J. Mater. Res.* **2015**, *30*, 93.
[39] A. H. Rahmati, S. Yang, S. Bauer, P. Sharma, *Soft Matter* **2019**, *15*, 127.
[40] F. Darbaniyan, K. Dayal, L. Liu, P. Sharma, *Soft Matter* **2019**, *15*, 262.
[41] Q. Deng, L. Liu, P. Sharma, *J. Mech. Phys. Solids* **2014**, *62*, 209.
[42] J. Nian, L. Chen, Z. Guo, W. Liu, *Friction* **2017**, *5*, 23.
[43] R. Gaillac, P. Pullumbi, F.- X. Coudert, *J. Phys.: Condens. Matter* **2016**, *28*, 275201.
[44] K. Z. Markov in *Heterogeneous Media* (Eds: K. Markov, L. Preziosi), Micromechanics Modeling Methods and Simulations, Engineering and Technology, Birkhäuser, Boston, MA, USA **2000**, pp. 1–162.
[45] A. Thyssen, *Charge Distribution and Stability in Electret Materials*, DTU Nanotech, Lyngby, Denmark **2016**.
[46] M. Dieterle, G. Mestl, *Phys. Chem. Chem. Phys.* **2002**, *4*, 822.
[47] H. I. Rasool, C. Ophus, A. Zettl, *Adv. Mater.* **2015**, *27*, 5771.
[48] Z. Lin, B. R. Carvalho, E. Kahn, R. Lv, R. Rao, H. Terrones, M. A. Pimenta, M. Terrones, *2D Mater.* **2016**, *3*, 022002.
[49] A. M. van der Zande, P. Y. Huang, D. A. Chenet, T. C. Berkelbach, Y. You, G.- H. Lee, T. F. Heinz, D. R. Reichman, D. A. Muller, J. C. Hone, *Nat. Mater.* **2013**, *12*, 554.
[50] A. Gruverman, S. V. Kalinin, in *Frontiers of Ferroelectricity* (Eds: S. B. Lang, H. L. W. Chan), Springer, Boston, MA, USA **2007**, pp. 107–116.
[51] S. V. Kalinin, S. Jesse, B. J. Rodriguez, K. Seal, A. P. Baddorf, T. Zhao, Y. H. Chu, R. Ramesh, E. A. Eliseev, A. N. Morozovska, B. Mirman, E. Karapetian, *Jpn. J. Appl. Phys.* **2007**, *46*, 5674.
[52] R. K. Vasudevan, S. Jesse, Y. Kim, A. Kumar, S. V. Kalinin, *MRS Commun.* **2012**, *2*, 61.
[53] S. Jesse, A. P. Baddorf, S. V. Kalinin, *Appl. Phys. Lett.* **2006**, *88*, 062908.
[54] J. S. Sekhon, L. Aggarwal, G. Sheet, *Appl. Phys. Lett.* **2014**, *104*, 162908.
[55] J. Yu, E. N. Esfahani, Q. Zhu, D. Shan, T. Jia, S. Xie, J. Li, *J. Appl. Phys.* **2018**, *123*, 155104.
[56] N. Balke, P. Maksymovych, S. Jesse, A. Herklotz, A. Tselev, C.-B. Eom, I. I. Kravchenko, P. Yu, S. V. Kalinin, *ACS Nano* **2015**, *9*, 6484.
[57] C. Ophus, *Adv. Struct. Chem. Imaging* **2017**, *3*, 13.
[58] A. Pryor, C. Ophus, J. Miao, *Adv. Struct. Chem. Imaging* **2017**, *3*, 15.

© 2020 WILEY-VCH Verlag GmbH & Co. KGaA, Weinheim